

# Effective Message Hiding with Order-Preserving Mechanisms

Gao Yu<sup>1</sup>

yu.gao2@cn.bosch.com

Qiu Xuchong\*<sup>1</sup>

xuchong.qiu@cn.bosch.com

Ye Zihan<sup>2</sup>

Zihan.Ye22@student.xjtlu.edu.cn

<sup>1</sup> Bosch ResearchBosch China Investment Ltd  
Shanghai, CN<sup>2</sup> Xi'an Jiaotong-Liverpool University  
Suzhou, CN

\* Corresponding Author

## Abstract

Message hiding, a technique that conceals secret message bits within a cover image, aims to achieve an optimal balance among message capacity, recovery accuracy, and imperceptibility. While Convolutional Neural Networks (CNNs) have notably improved message capacity and imperceptibility, obtaining high recovery accuracy remains challenging. This arises because, in contrast to image data, the sequential arrangement of message bits is imperative, but convolutional operations encounter inherent difficulties in preserving this critical order. In addition, CNNs also struggle to effectively address the large discrepancy between these two uncorrelated modalities. To address this, we propose StegaFormer, an innovative MLP-based framework designed to preserve bit order and enable global fusion between modalities. Specifically, StegaFormer incorporates three crucial components: Order-Preserving Message Encoder (OPME), Order-Preserving Message Decoder (OPMD), and Global Message-Image Fusion (GMIF). OPME and OPMD aim to preserve the order of message bits by segmenting the entire sequence into equal-length segments and incorporating sequential information during encoding and decoding. Meanwhile, GMIF employs a cross-modality fusion mechanism to effectively fuse the features from the two uncorrelated modalities. Experimental results on the COCO and DIV2K datasets demonstrate that StegaFormer significantly outperforms existing state-of-the-art methods in terms of recovery accuracy, message capacity, and imperceptibility. Our code is released in <https://github.com/boschresearch/Stegaformer>.

## 1 Introduction

Image steganography is a technique that conceals confidential information within a publicly accessible image [20, 22, 25, 36]. In this study, we focus on message hiding. It has a wide range of applications such as copy-right protection, light field messaging [32], virtual reality and augmented reality applications [26] and face anonymization [14]. The goal of it is embedding secret message bits within a cover image to produce a new image (called stego

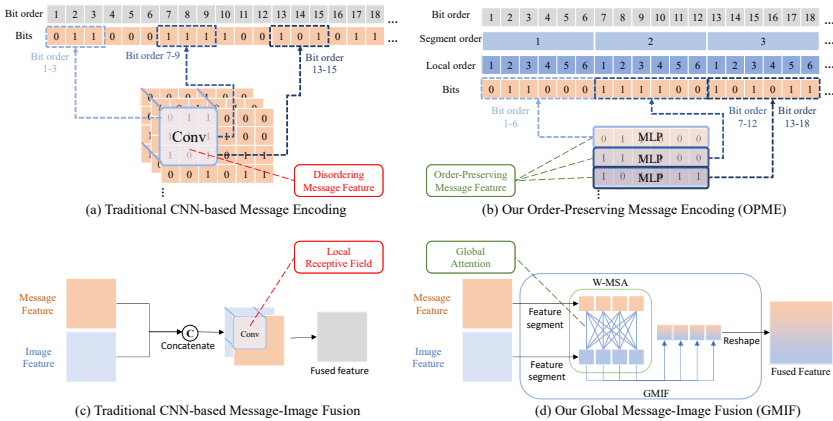


Figure 1: The illustration of our proposed methods. (a) CNN-based message encoding that disorders the message bits in message encoding and (b) our proposed message encoding: Order-Preserving Message Encoder (OPME) that preserves the order of message bits by segmenting and MLP-based encoding. (c) CNN-based message-image feature fusion and (d) our proposed message-image fusion using Global Message-Image Fusion (GMIF).

image). Ensuring a balanced trade-off among message capacity, recovery accuracy, and imperceptibility is the core task. More concretely, message capacity is measured by bits per pixel (BPP). Recovery accuracy indicates the message fidelity after being processed by these methods. Imperceptibility is minimizing the perceptible differences between the cover image and the stego image. It’s usually measured by the image quality metrics such as peak signal-to-noise ratio (PSNR) and structural similarity index (SSIM) [34].

Traditional message hiding methods often rely on heuristic approaches, such as the Least Significant Bit method [20], which modifies individual pixels of a digital image to conceal message bits. Recently, with the advancements of deep learning, Convolutional Neural Network (CNN) based methods have significantly improved the message capacity and imperceptibility [25, 31, 33, 35, 36]. These methods involve aligning and concatenating message bits with the cover image in a spatial manner while utilizing CNNs to seamlessly integrate the message and image.

However, CNN-based approaches often yield suboptimal results in message encoding and recovery, particularly when employing convolutional operations to encode multiple layers of message bits (message capacity > 1 BPP) as illustrated in Fig. 1(a). We have identified two main limitations in current CNN-based methods. Firstly, the indiscriminate use of convolutional kernels to encode message bits disrupts the sequential order of the original message bits. Secondly, the element-wise concatenation of message and image features, followed by convolutional operations, underestimates the substantial disparity between these two uncorrelated modalities, resulting in inadequate fusion as shown in Fig. 1(c).

To validate these assumptions, we gradually modified the kernel size of SteganoGAN [36] and ChatGAN [25] in the experiments using DIV2K [10] dataset at 4 BPP message capacity, as this capacity represents the boundary where message hiding accuracy starts to drop below 90%. The experiments shows, reducing the kernel size leads to improved message recovery accuracy. Decreasing the kernel size from 7 to 1 simplifies the 2D convolution layers to Multi-Layer Perceptrons (MLPs), focusing on single-bit or multi-bit 1D message segment features along the channel dimension at higher BPPs. The encoded 1D message segments

are then sequentially encoded along the spatial dimensions, preserving the original bit string order by dividing it into smaller segments. Conversely, increasing the kernel size enhances stego image quality by enlarging the receptive field, facilitating global interactions between message and image features. Our assumption is that the early convolution modules focus on message encoding, while later stages prioritize message-image fusion, as the message bits are typically concatenated with image features at the beginning. Further experimental details are provided in the supplementary material.

To address these challenges, as shown in Fig. 1(b), we leverage on MLP to design a more appropriate method for message encoding. The MLP-based message encoding phase can maintain the local order of small message segments. And the Multi-Head Self-Attention (MHSA) [28] and positional embeddings (PEs) help to encode the message features while explicitly adding global order information to the encoded message features. In this context, “local” refers to the order within a message segment, while “global” refers to the sequential order of the message segments. For message and image fusion, as shown in Fig. 1(d), we use Windowed Multi-Head Self-Attention Layer (W-MSA) to address the limitation of receptive fields in the CNN-based structure, enabling global interactions between the uncorrelated message and image features.

Our proposed approach, named StegaFormer, consists of three modules for enhanced message encoding, decoding, and message-image fusion, respectively. We design the first two modules, Order-Preserving Message Encoder (OPME) and Order-Preserving Message Decoder (OPMD), to effectively handle message segments while preserving their order. The OPMD adopts a symmetric structure and methodology with OPME for decoding. Additionally, OPME and OPMD fully leverage sequential order by incorporating PEs into the message features and globally encoding and decoding the features using MHSA. The last module, Global Message-Image Fusion (GMIF), employs Windowed Multi-Head Self-Attention Layer (W-MSA) [19] to globally fuse the information from the secret message and cover image into the stego image, greatly minimizing perceptible artifacts in the stego image.

Our contributions are summarized as follows: (1) We are the first to explore the limitations of message hiding using CNN-based architecture; consequently, we transfer to an MLP-based approach design. (2) We introduce two novel modules OPME & OPMD, which enhance the message encoding and decoding by incorporating sequential order into the message. (3) We design GMIF, which leverages the global interaction of W-MSA to effectively fuse secret message and cover image features to stego image features. (4) Experimental results on real-world datasets demonstrate the superiority of our framework over existing state-of-the-art methods in terms of accuracy, capacity, and imperceptibility.

## 2 Related Work

**Message Hiding.** Traditional methods often involve altering individual pixels in an image using heuristic techniques. They generally have a high recovery accuracy and imperceptibility, but low capacity. Specifically, early studies [20, 22] manipulate the least significant bits of the cover image. Others [9, 7, 12, 24] extend this approach to the frequency domain by transforming the cover image to different types of frequency domains for better performance. Despite their capacity for precise secret message recovery, these methods can only hide an extremely low BPP (*i.e.*, 0.4) to evade detection by steganalysis tools [11, 13].

Recently, CNN-based methods for message hiding have significantly improved capacity and gained considerable attention [8, 23, 63, 66]. For instance, SteganoGAN [56] introduced

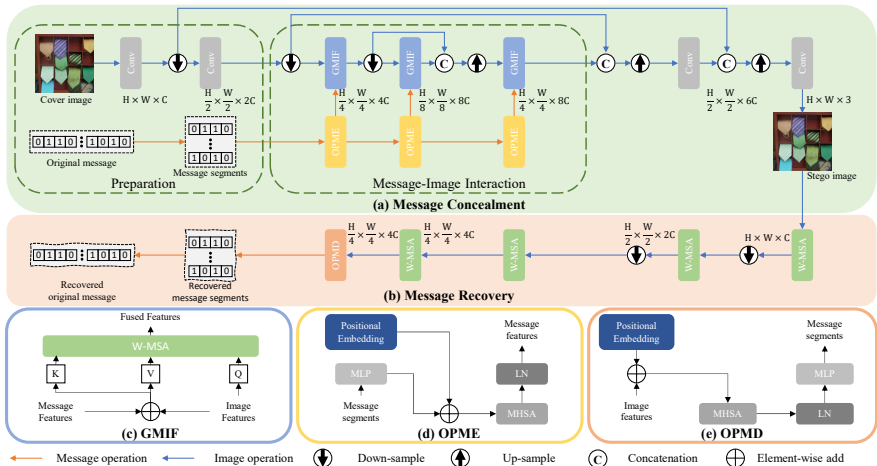


Figure 2: The overview of StegaFormer consists of two main pipelines: (a) Message Concealment and (b) Message Recovery, which are facilitated by three proposed components: (c) Global Message-Image Fusion (GMIF), (d) Order-Preserving Message Encoder (OPME), and (e) Order-Preserving Message Decoder (OPMD). The sizes indicated above the modules represent the shapes of their respective outputs. LN denotes Layer Normalization.

3D message tensor alignment along spatial dimensions with the image tensor, and ChatGAN [25] incorporated channel attention to enhance accuracy and imperceptibility while maintaining high capacity. SFTN [83] was proposed to address rounding errors before generating the stego image. However, these CNN-based approaches contribute little to improving message recovery accuracy.

To address this issue, other works [9, 14] employ offline optimization, directly optimizing the stego image itself by iteratively adding adversarial perturbations to it. We refer to this approach as the iterative method, in contrast with the previous approaches, termed non-iterative methods. While this iterative approach can improve message hiding accuracy, it requires additional optimization steps for each image during both training and inference, leading to an inference time exceeding 600 ms per image and significantly compromising the imperceptibility.

Inspired by the difficulties encountered in previous works, we now turn our attention to the details of the message encoding procedure in these CNN-based models. We reveal their main constraint: CNNs disorder the message order, thus having limited accuracy. Thus, differing from previous CNN-based methods, we are the first to leverage MLPs, MHSA and PEs to design an order-preserving framework.

**Multi-head Self-Attention.** Attention mechanism is widely adopted in the domain of Natural Language Processing [27] and various computer vision tasks [8, 6, 15, 23, 69]. The benefits of it stem from the dynamic weights and long-range encoding capability [13]. We adopt the W-MSA [19] as the fundamental building block of the message-image fusion, enabling long contextual fusion of message and image features with less computational complexity.

### 3 Methods

As illustrated in Fig. 2, our proposed method encompasses two pipelines for message concealment, *i.e.*, Fig. 2(a), and message recovery, *i.e.*, Fig. 2(b), respectively. This approach

sets itself apart from previous works by incorporating three crucial components: the GMIF, as depicted in Fig. 2(c), for the fusion between features from the secret message and cover image, the OPME, as shown in Fig. 2(d), for order-preserving message encoding, OPMD as shown in Fig. 2(e) for corresponding message decoding.

## 3.1 Preparation

### 3.1.1 Message Layout Preparation

A secret message  $M \in \{0, 1\}^L$ , consisting of  $L$  bits, is structured in the form  $M \in \{0, 1\}^{H \times W \times D}$  in previous approaches [9, 25, 33, 36]. Here,  $H$  and  $W$  represent the spatial dimensions of the message tensor, which correspond to the height and width of the cover image, while  $D$  denotes the message capacity (e.g.,  $D = 1$  for 1 BPP message capacity). Although this message layout can be easily processed using convolutional layers, it does introduce inappropriate limitations, as discussed in Sec. 1.

To address the issue, we introduce an unique message layout to introducing sequential order in the raw message bits. In this message layout, the message  $M \in \{0, N_r\}^L$  is represented as  $M_{\text{seg}} \in \{0, N_r\}^{N_{\text{ms}} \times L_{\text{ms}}}$  where  $N_{\text{ms}} \times L_{\text{ms}} = L$ . Here,  $N_r$  denotes the range of message elements and  $N_{\text{ms}}$  represents the number of message segments,  $L_{\text{ms}}$  is the length of each message segments, and  $L_{\text{ms}} \ll L$ . Unless stated otherwise,  $N_r$  is set to 1, as in previous approaches. We further explore expanding  $N_r$  from 0 to 1 to higher ranges, such as 0 to 3 (representing 2 bits per message element), for high message capacity modes. Considering the multi-level structure of StegaFormer, we configure  $N_{\text{ms}}$  and  $L_{\text{ms}}$  at different sizes to align with the shape of the corresponding image features.

### 3.1.2 Image Feature Preparation

Our model adopt 2D convolution as image feature extractor. Given a cover image  $I_{\text{cover}} \in \mathbb{R}^{H \times W \times 3}$ , where  $H$  and  $W$  represent the height and width of the cover image, we employ two stages of operations to extract image feature  $F_{\text{im}} \in \mathbb{R}^{(H/2^i \times W/2^i) \times 2^i \times C}$ . Here,  $i = 1, 2$  indicates the number of stages, and  $C$  is the number of channels in the output feature. For models with different message capacities, we set  $C = 2 \times L_{\text{ms}}$ . Each stage consists of 2D convolution layers followed by a down-sampling operation. The down-sampling operation applies convolution to reduce the spatial size of the feature map by half while doubling its feature depth. The output of the image feature preparation phase is  $F_{\text{im}} \in \mathbb{R}^{(H/4 \times W/4) \times 4C}$ .

## 3.2 Order-Preserving Modules

### 3.2.1 Order-Preserving Message Encoder

The main challenge in message encoding lies in effectively converting secret message bits into message features while retaining the sequential information of the message. To address this, we propose an OPME that efficiently encodes the message while preserving both local and global sequential information. Our model consists of three OPME in total to enable multi-scale interaction between the message and image features.

Each OPME incorporates an MLP, referred to as  $\text{MLP}_{\text{enc}}$ , which functions as a channel encoder. Its purpose is to encode message segments  $M_{\text{seg}} \in \{0, 1\}^{N_{\text{ms}} \times L_{\text{ms}}}$  into message

feature  $F_{\text{msg}}$  following Eq. (1):

$$F_{\text{msg}} = \text{MLP}_{\text{enc}}(M_{\text{seg}}), \quad (1)$$

where the depth of  $F_{\text{msg}}$  is greater than  $L_{\text{ms}}$  and the shape of  $F_{\text{msg}}$  is equal to the shape of  $F_{\text{im}}$  at the corresponding GMIF. This learning-based channel encoder [21] introduces redundant code into the original message segments, facilitating the stable transmission of the message feature within the model.

The importance of maintaining the sequential order of message segments is highlighted by the incorporation of PEs into the encoded segments. This is demonstrated in Eq. (2):

$$F_{\text{msg}}^{\text{global}} = \text{LN}(\text{MHSA}(F_{\text{msg}} + E_{\text{pos}})), \quad (2)$$

where positional embedding  $E_{\text{pos}}$  is introduced to the  $F_{\text{msg}}$  followed by a MHSA module [22] to globally encode  $F_{\text{msg}}$  to  $F_{\text{msg}}^{\text{global}}$ . Layer Normalization (LN) [23] is employed to normalize the global message features. We further validate effectiveness of PEs in Sec. 4.4.

### 3.2.2 Order-Preserving Message Decoder

As depicted in Fig. 2(b), we employ a standard SwinTransformer [18] with minor modifications to extract features from  $I_{\text{stego}}$ . Specifically, the down-sampling operations in the last two layers of the W-MSA module within SwinTransformer are removed to match the spatial size to the feature of the secret message in the OPME. Subsequently, the OPMD reconstructs the secret message segments  $\hat{M}$  from the extracted features. The OPMD follows the same methodology as the OPME, but in reverse order.

### 3.3 Global Message-Image Fusion

Our GMIF, as shown in Eq. (3):

$$F_{\text{stego}} = \text{GMIF}(F_{\text{msg}}^{\text{global}}, F_{\text{im}}), \quad (3)$$

is designed to accomplish two fundamental goals of message hiding. These goals encompass: (1) the stego image should contain all the information from both the secret message and the cover image; (2) the ideal stego image should be nearly identical to the cover image. The key, value and query in the attention mechanism are configured according to these two goals to translate the message and image information to the steganographic features where the key, value and query are set as:  $K = (F_{\text{im}} + F_{\text{msg}}^{\text{global}})W^K$ ,  $V = (F_{\text{im}} + F_{\text{msg}}^{\text{global}})W^V$ , and  $Q = F_{\text{im}}W^Q$ . This configuration utilized in our approach are inspired by the Transformer-based architecture commonly employed in language translation tasks. Drawing a parallel, we apply a similar mechanism to the task of message hiding, as both involve dealing with a lack of spatial and semantic alignment between the secret message and cover image. The GMIF-effectively fuses the optimal stenographic information, which is the sum of  $F_{\text{msg}}^{\text{global}}$  and  $F_{\text{im}}$ , into the desired feature representation of the stego image  $F_{\text{stego}}$ . More details related to the key, value, and query of GMIF are provided in the supplementary material.

The basic building block of GMIF is W-MSA. One layer of W-MSA with large window size is applied to ensure a comprehensive global interaction between message and image features in the GMIF. We apply up-sampling and convolution layers to the concatenated  $F_{\text{stego}}$

Dataset	COCO									
Metric	ACC			PSNR			SSIM			Inference Time
Capacity	1 BPP	2 BPP	3 BPP	1 BPP	2 BPP	3 BPP	1 BPP	2 BPP	3 BPP	ms
LISO* [9]	99.99%	99.98%	99.84%	33.67	33.40	28.20	0.9424	0.9350	0.8184	607.7
SteganoGAN [16]	97.75%	96.46%	91.35%	42.52	39.68	36.45	0.9894	0.9801	0.9650	1.6
ChatGAN [15]	99.07%	97.46%	96.18%	46.42	43.17	41.84	0.9943	0.9880	0.9832	3.0
StegaFormer (Ours)	<b>99.95%</b>	<b>99.85%</b>	<b>99.68%</b>	<b>47.83</b>	<b>45.30</b>	<b>43.37</b>	<b>0.9969</b>	<b>0.9943</b>	<b>0.9914</b>	9.1

Dataset	DIV2K									
Metric	ACC			PSNR			SSIM			Inference Time
Capacity	1 BPP	2 BPP	3 BPP	1 BPP	2 BPP	3 BPP	1 BPP	2 BPP	3 BPP	ms
LISO* [9]	99.91%	99.83%	99.55%	35.52	33.67	30.13	0.9394	0.9088	0.8326	607.7
SteganoGAN [16]	98.96%	97.63%	92.23%	39.36	37.97	36.14	0.9793	0.8916	0.8343	1.6
ChatGAN [15]	99.73%	98.63%	94.75%	45.00	42.05	40.63	0.9929	0.9861	0.9782	3.0
StegaFormer (Ours)	<b>99.94%</b>	<b>99.87%</b>	<b>99.76%</b>	<b>51.98</b>	<b>49.07</b>	<b>47.31</b>	<b>0.9985</b>	<b>0.9970</b>	<b>0.9958</b>	9.1

Table 1: Quantitative comparisons of different approaches with ours on the COCO and DIV2K datasets are presented. ACC denotes message recovery accuracy, while PSNR and SSIM are two metrics to measure the level of imperceptibility. The best results for non-iterative methods are highlighted in bold. \* denotes iterative method.

and  $F_{\text{im}}$  to reconstruct the residual image  $I_{\text{res}}$ . The up-sampling layer uses a de-convolution operation to double the height and width of the feature map and reduce the feature dimension by half. The final output of our model is  $I_{\text{stego}}$ , which is equal to the sum of  $I_{\text{cover}}$  and  $I_{\text{res}}$ . Please check supplementary material for detailed configurations of our model.

### 3.4 Loss Function

The objectives of message hiding are two-fold: to generate a stego image that closely resembles the cover image and to precisely retrieve the secret message from the stego image. In pursuit of these aims, we employ the loss function defined as  $\mathcal{L}_{\text{total}} = \mathcal{L}_{\text{img}} + \mathcal{L}_{\text{msg}}$ , where  $\mathcal{L}_{\text{img}} = \lambda_1 \mathcal{L}_{\text{MSE}}(I_{\text{cover}}, I_{\text{stego}}) + \lambda_2 \mathcal{L}_{\text{LPIPs}}(I_{\text{cover}}, I_{\text{stego}})$  where LPIPs [67] is perceptual loss, and  $\mathcal{L}_{\text{msg}} = \mathcal{L}_{\text{BCE}}(M, \hat{M})$  if the range of message  $N_r = 1$ , or  $\mathcal{L}_{\text{msg}} = \mathcal{L}_{\text{MSE}}(M, \hat{M})$  if the message range  $N_r > 1$ .

## 4 Experiments

To demonstrate the effectiveness of our proposed approach, we conduct a comparative analysis of message recovery accuracy and imperceptibility against three state-of-the-art message hiding methods. SteganoGAN [16], ChatGAN [15] are non-iterative approaches and LISO [9] is iterative. This analysis is carried out across different message capacity levels.

Following previous studies [9, 15, 16], our method is evaluated on two public datasets: COCO [17] and DIV2K [18]. The COCO dataset for message hiding contains 25,000 images randomly sampled from the original COCO training split for model training, as well as 500 images randomly sampled from the original COCO test split for model evaluation. No extra configurations for DIV2K dataset. All images are center cropped to  $256 \times 256$  pixels. Three metrics are used to evaluate the model performance. The message recovery accuracy is utilized to assess the percentage of successfully recovered secret messages. The imperceptibility of stego images is measured using the PSNR and SSIM. More detailed configurations of our model are listed in the supplementary material due to the page limitation.



Figure 3: Qualitative results of 3 BPP message hiding using different methods: (a) SteganoGAN, (b) ChatGAN and (c) Ours.  $I_{cover}$ ,  $I_{stego}$  and  $I_{res}$  represent cover image, stego image and residual image respectively.

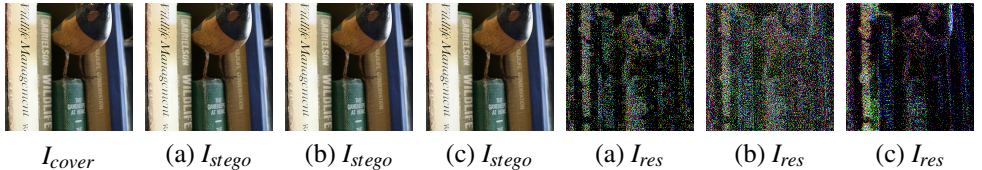


Figure 4: Qualitative results of high-capacity message hiding with our method: (a) 4 BPP, (b) 6 BPP and (c) 8 BPP.  $I_{cover}$ ,  $I_{stego}$  and  $I_{res}$  represent cover image, stego image and residual image respectively.

## 4.1 Comparison with State-of-the-Art Methods

We conducted a comprehensive comparison between our method and two existing non-iterative message hiding methods, namely SteganoGAN [56] and ChatGAN [25], as well as the latest iterative method LISO [9]. As summarized in Tab. 1, our method consistently outperforms the non-iterative methods in terms of recovery accuracy and imperceptibility across different message capacities (1, 2, and 3 BPP). Specifically, at a 3 BPP capacity, our method achieves impressive recovery accuracies of 99.68% and 99.76% for the COCO and DIV2K datasets, respectively. These results represent significant improvements of 3.5% and 5.0% over the current non-iterative state-of-the-art accuracies achieved by ChatGAN, demonstrating the effectiveness of our approach (OPME) in achieving high-accuracy message hiding. In contrast to the iterative method, our approach achieves comparable levels of message recovery accuracy. Notably, our method outperforms the accuracy of iterative approach when trained on high quality image datasets such as DIV2K.

Furthermore, our method enhances imperceptibility in terms of both PSNR and SSIM across different message capacities. It achieve much higher quality than iterative method since this approach significantly hinder the quality of stego image. Compared with the best non-iterative method ChatGAN, at a 3 BPP message capacity, our method improves the PSNR from 41.84 to 43.37 on the COCO dataset and from 40.63 to 47.31 on the DIV2K dataset. These results underscore the effectiveness of our approach (GMIF) in fusing steganographic information into stego images, achieving significantly higher imperceptibility than the iterative method. In terms of inference time, our method achieves similar levels of efficiency as other non-iterative approaches. In contrast, iterative methods such as LISO typically require over 600 ms due to the extra iterations during inference.

Fig. 3 illustrates a cover image (a), stego images (b) to (d) generated by our method and previous methods [25, 56] at 3 BPP message capacity, and residual images (e) to (g). All the pixel values of residual images are enlarged by 5 times. The residual images produced by our method demonstrate that minimal changes have been applied to the cover images. In contrast, previous approaches introduce higher residuals throughout the cover image, resulting in lower imperceptibility. More qualitative results are in the supplementary material.



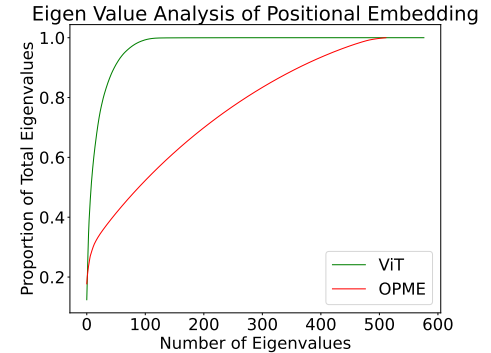
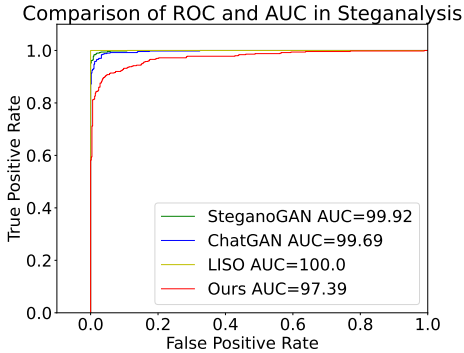


Figure 5: Detection accuracy of different methods. Lower is better.

Figure 6: The eigen values analysis of PEs from ViT and OPME.

BPP	4	6	8
ACC (%)	99.27	96.65	91.78
PSNR	41.87	40.37	34.70
SSIM	0.9877	0.9803	0.9508

Table 2: StegaFormer results at large BPPs.

Model	ACC	PSNR	SSIM
Baseline	50.01	53.4	0.9988
+GMIF	87.60	43.78	0.9908
+GMIF+OPME+OPMD	<b>99.24</b>	<b>41.78</b>	<b>0.9875</b>

Table 3: Ablation of OPME, OPMD and GMIF.

## 4.2 Models for High Message Capacity

We conduct a series of experiments to showcase the performance of our method in handling high message capacities. As shown in Tab. 2, the results demonstrate that our method achieves more than 90% message recovery accuracy for message capacities up to 8 BPP. Compared with existing methods, these results highlight the remarkable improvements of our method in both message capacity and recovery accuracy. Besides, Fig. 4 (b) to (g) depicts the stego and residual images by our models with high message capacities. The residual images of these high-capacity models demonstrate the outstanding imperceptibility of our models. Please check the supplementary material for details related to large message capacity models.

## 4.3 Steganalysis

Steganalysis methods [9, 34, 35] play a crucial role in assessing the security of stego images. In our study, we choose the state-of-the-art steganalysis approach SiaStegNet [34] to conduct a comprehensive benchmark comparison between our method and existing methods [9, 25, 36]. Fig. 5 presents the steganalysis results on COCO dataset, demonstrating that our model achieves the lowest Area Under the Curve (AUC) among the three compared methods. These results indicate that our method exhibits the lowest detection rate and has the best security of stego images. All message hiding models for comparison have a 3 BPP message capacity. More details of steganalysis are in the supplementary material.

## 4.4 Ablation Study

To prove the effectiveness of our purposed components. We first evaluate the performance of OPME, OPMD and GMIF. Later, go into the details of the OPME and OPMD. As shown in Tab. 3, we evaluate the efficacy of our order-preserving mechanism in OPME and OPMD, as well as the global interaction design in GMIF, by progressively scaling down our model. We do this by gradually removing OPME, OPMD, and GMIF to establish a baseline model, and then conducting message hiding training using COCO with a 4 BPP payload. In the absence of these components 2D convolution layers are utilized. It becomes apparent that the absence of both OPME and OPMD, as well as GMIF, hinders the model’s ability to effectively hide the secret message within the cover image. A model employing only GMIF can enhance accuracy through more efficient message-image fusion. However, the inclusion of OPME and OPMD substantially improves message recovery accuracy, underscoring the importance of preserving the sequential order of the message during encoding.

As illustrated in Tab. 4, we evaluate the effectiveness of internal modules of OPME and OPMD at 4 BPP using the COCO dataset. We begin by testing models containing only an MLP and gradually add MHSA and PEs. The inclusion of solely PEs or MHSA after the MLP module yields suboptimal performances. The optimal performance is achieved with the default design of our OPME and OPMD, which incorporates MLP, MHSA, and PEs.

To further validate whether OPME and OPMD effectively model the independent nature of message segments, we analyze the ratio between the cumulative sum of the top  $n$  eigenvalues and the sum of all eigenvalues of PEs [29]. Specifically, we compare this characteristic of PEs obtained from ViT with those from OPME. As shown in Fig. 6, positional embeddings from ViT display significant eigenvalues, suggesting shared positional information among numerous image patches for image classification tasks. In contrast, PEs from OPME lack prominent eigenvalues, indicating much greater independence of positional information. This demonstrates that OPME effectively assigns distinct positional information to individual message segments.

MLP	MHSA	PE	ACC	PSNR	SSIM
✓	×	×	98.59	40.59	0.9826
✓	✓	×	98.68	40.70	0.9833
✓	×	✓	97.92	40.05	0.9786
✓	✓	✓	<b>99.24</b>	<b>41.78</b>	<b>0.9875</b>

Table 4: Ablation of components of OPME and OPMD.

## 5 Conclusion

We propose StegaFormer, a novel message hiding framework for high accuracy message concealment and recovery. StegaFormer is able to increase the message recovery accuracy by emphasizing the order of message bits and cross-modality feature fusion. Experiments on real-world datasets demonstrate that our method consistently outperforms the SOTA methods in terms of message recovery accuracy, message capacity, and imperceptibility.

## References

- [1] Eirikur Agustsson and Radu Timofte. Ntire 2017 challenge on single image super-resolution: Dataset and study. In *Proceedings of the IEEE conference on computer vision and pattern recognition workshops*, pages 126–135, 2017.
- [2] Jimmy Lei Ba, Jamie Ryan Kiros, and Geoffrey E Hinton. Layer normalization. *arXiv preprint arXiv:1607.06450*, 2016.
- [3] Xuyang Bai, Zeyu Hu, Xinge Zhu, Qingqiu Huang, Yilun Chen, Hongbo Fu, and Chiew-Lan Tai. Transfusion: Robust lidar-camera fusion for 3d object detection with transformers. In *Proceedings of the IEEE/CVF conference on computer vision and pattern recognition*, pages 1090–1099, 2022.
- [4] Ning Bi, Qiyu Sun, Daren Huang, Zhihua Yang, and Jiwu Huang. Robust image watermarking based on multiband wavelets and empirical mode decomposition. *IEEE Transactions on Image Processing*, 16(8):1956–1966, 2007.
- [5] Mehdi Boroumand, Mo Chen, and Jessica Fridrich. Deep residual network for steganalysis of digital images. *IEEE Transactions on Information Forensics and Security*, 14(5):1181–1193, 2018.
- [6] Nicolas Carion, Francisco Massa, Gabriel Synnaeve, Nicolas Usunier, Alexander Kirillov, and Sergey Zagoruyko. End-to-end object detection with transformers. In *ECCV*, pages 213–229. Springer, 2020.
- [7] Rajarathnam Chandramouli, Mehdi Kharrazi, and Nasir Memon. Image steganography and steganalysis: Concepts and practice. In *International Workshop on Digital Watermarking*, pages 35–49. Springer, 2003.
- [8] Xiangyu Chen, Varsha Kishore, and Kilian Q Weinberger. Learning iterative neural optimizers for image steganography. In *The Eleventh International Conference on Learning Representations*, 2022.
- [9] Xiangyu Chen, Varsha Kishore, and Kilian Q Weinberger. Learning iterative neural optimizers for image steganography. In *The Eleventh International Conference on Learning Representations*, 2023. URL <https://openreview.net/forum?id=gLPkzWjdhBN>.
- [10] Jessica Fridrich and Jan Kodovsky. Rich models for steganalysis of digital images. *IEEE Transactions on information Forensics and Security*, 7(3):868–882, 2012.
- [11] Miroslav Goljan, Jessica Fridrich, and Taras Holotyak. New blind steganalysis and its implications. In *Security, Steganography, and Watermarking of Multimedia Contents VIII*, volume 6072, page 607201. International Society for Optics and Photonics, 2006.
- [12] Vojtěch Holub and Jessica Fridrich. Designing steganographic distortion using directional filters. In *2012 IEEE International workshop on information forensics and security (WIFS)*, pages 234–239. IEEE, 2012.
- [13] Salman Khan, Muzammal Naseer, Munawar Hayat, Syed Waqas Zamir, Fahad Shahbaz Khan, and Mubarak Shah. Transformers in vision: A survey. *ACM computing surveys (CSUR)*, 54(10s):1–41, 2022.

- [14] Varsha Kishore, Xiangyu Chen, Yan Wang, Boyi Li, and Kilian Q Weinberger. Fixed neural network steganography: Train the images, not the network. In *International Conference on Learning Representations*, 2021.
- [15] Yingwei Li, Adams Wei Yu, Tianjian Meng, Ben Caine, Jiquan Ngiam, Daiyi Peng, Junyang Shen, Yifeng Lu, Denny Zhou, Quoc V Le, et al. Deepfusion: Lidar-camera deep fusion for multi-modal 3d object detection. In *Proceedings of the IEEE/CVF Conference on Computer Vision and Pattern Recognition*, pages 17182–17191, 2022.
- [16] Tingting Liang, Hongwei Xie, Kaicheng Yu, Zhongyu Xia, Zhiwei Lin, Yongtao Wang, Tao Tang, Bing Wang, and Zhi Tang. Bevfusion: A simple and robust lidar-camera fusion framework. *Advances in Neural Information Processing Systems*, 35:10421–10434, 2022.
- [17] Tsung-Yi Lin, Michael Maire, Serge Belongie, James Hays, Pietro Perona, Deva Ramanan, Piotr Dollár, and C Lawrence Zitnick. Microsoft coco: Common objects in context. In *European conference on computer vision*, pages 740–755. Springer, 2014.
- [18] Ze Liu, Yutong Lin, Yue Cao, Han Hu, Yixuan Wei, Zheng Zhang, Stephen Lin, and Baining Guo. Swin transformer: Hierarchical vision transformer using shifted windows. In *ICCV*, pages 10012–10022, 2021.
- [19] Ze Liu, Han Hu, Yutong Lin, Zhuliang Yao, Zhenda Xie, Yixuan Wei, Jia Ning, Yue Cao, Zheng Zhang, Li Dong, et al. Swin transformer v2: Scaling up capacity and resolution. In *Proceedings of the IEEE/CVF conference on computer vision and pattern recognition*, pages 12009–12019, 2022.
- [20] Jarno Mielikainen. Lsb matching revisited. *IEEE signal processing letters*, 13(5): 285–287, 2006.
- [21] Timothy O’shea and Jakob Hoydis. An introduction to deep learning for the physical layer. *IEEE Transactions on Cognitive Communications and Networking*, 3(4):563–575, 2017.
- [22] Tomáš Pevný, Tomáš Filler, and Patrick Bas. Using high-dimensional image models to perform highly undetectable steganography. In *International Workshop on Information Hiding*, pages 161–177, 2010.
- [23] René Ranftl, Alexey Bochkovskiy, and Vladlen Koltun. Vision transformers for dense prediction. In *ICCV*, pages 12179–12188, 2021.
- [24] HS Manjunatha Reddy and KB Raja. High capacity and security steganography using discrete wavelet transform. *International Journal of Computer Science and Security (IJCSS)*, 3(6):462, 2009.
- [25] Jingxuan Tan, Xin Liao, Jiatae Liu, Yun Cao, and Hongbo Jiang. Channel attention image steganography with generative adversarial networks. *IEEE Transactions on Network Science and Engineering*, 2021.
- [26] Matthew Tancik, Ben Mildenhall, and Ren Ng. Stegastamp: Invisible hyperlinks in physical photographs. In *CVPR*, 2020.

- [27] Ashish Vaswani, Noam Shazeer, Niki Parmar, Jakob Uszkoreit, Llion Jones, Aidan N Gomez, Łukasz Kaiser, and Illia Polosukhin. Attention is all you need. In *Advances in Neural Information Processing Systems*, volume 30, 2017.
- [28] Ashish Vaswani, Noam Shazeer, Niki Parmar, Jakob Uszkoreit, Llion Jones, Aidan N Gomez, Łukasz Kaiser, and Illia Polosukhin. Attention is all you need. *Advances in neural information processing systems*, 30, 2017.
- [29] Yu-An Wang and Yun-Nung Chen. What do position embeddings learn? an empirical study of pre-trained language model positional encoding. In *Proceedings of the 2020 Conference on Empirical Methods in Natural Language Processing (EMNLP)*, pages 6840–6849, 2020.
- [30] Zhou Wang, Alan C Bovik, Hamid R Sheikh, and Eero P Simoncelli. Image quality assessment: from error visibility to structural similarity. *IEEE transactions on image processing*, 13(4):600–612, 2004.
- [31] Ping Wei, Sheng Li, Xinpeng Zhang, Ge Luo, Zhenxing Qian, and Qing Zhou. Generative steganography network. In *Proceedings of the 30th ACM International Conference on Multimedia*, pages 1621–1629, 2022.
- [32] Eric Wengrowski and Kristin Dana. Light field messaging with deep photographic steganography. In *CVPR*, 2019.
- [33] Xiaolin Yin, Shaowu Wu, Ke Wang, Wei Lu, Yicong Zhou, and Jiwu Huang. Anti-rounding image steganography with separable fine-tuned network. *IEEE Transactions on Circuits and Systems for Video Technology*, 2023.
- [34] Weike You, Hong Zhang, and Xianfeng Zhao. A siamese cnn for image steganalysis. *IEEE Transactions on Information Forensics and Security*, 16:291–306, 2020.
- [35] Chong Yu. Attention based data hiding with generative adversarial networks. In *Proceedings of the AAAI conference on artificial intelligence*, volume 34, pages 1120–1128, 2020.
- [36] Kevin Alex Zhang, Alfredo Cuesta-Infante, and Kalyan Veeramachaneni. Steganogan: High capacity image steganography with gans. *arXiv preprint arXiv:1901.03892*, 2019. URL <https://arxiv.org/abs/1901.03892>.
- [37] Richard Zhang, Phillip Isola, Alexei A Efros, Eli Shechtman, and Oliver Wang. The unreasonable effectiveness of deep features as a perceptual metric. In *CVPR*, pages 586–595, 2018.
- [38] Ru Zhang, Feng Zhu, Jianyi Liu, and Gongshen Liu. Depth-wise separable convolutions and multi-level pooling for an efficient spatial cnn-based steganalysis. *IEEE Transactions on Information Forensics and Security*, 15:1138–1150, 2019.
- [39] Xizhou Zhu, Weijie Su, Lewei Lu, Bin Li, Xiaogang Wang, and Jifeng Dai. Deformable detr: Deformable transformers for end-to-end object detection. In *International Conference on Learning Representations*, 2020.

## Supplementary Material for Effective Message Hiding with Order Preserving Mechanisms

This appendix is organized as follows.

- A. Details of the kernel size experiment conducted using SteganoGAN [56] and ChatGAN [25].
- B. Experiments investigating the selection of keys, values, and queries for GMIF.
- C. The detailed configuration of StegaFormer.
- D. Detailed settings for the quantitative experiment.
- E. Additional qualitative comparisons between StegaFormer and previous approaches [25, 56]. Qualitative examples for our models from 1 BPP to 8 BPP.
- F. Detailed settings for steganalysis experiments.

### A Kernel Size Experiment

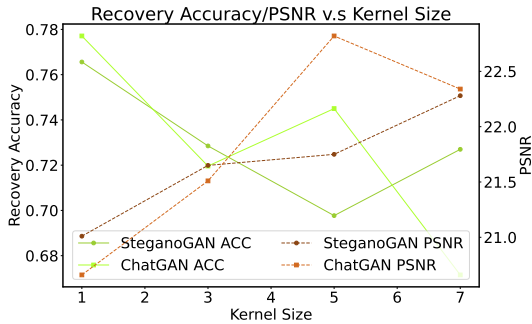


Figure 7: The effects of different kernel size to the recovery accuracy and imperceptibility.

As depicted in Fig. 7, we conduct several experiments related to the kernel size of the CNN-based approach to investigate its limitations. The experiments for SteganoGAN [56] is based on the officially released code. We choose the base model of SteganoGAN as it avoids the complexities of other variants that involve embedding messages at multiple convolutional stages, making it difficult to discern how message features are encoded into the image features. Since there is no official code released for ChatGAN [25], our experiments for this approach is based on our own implementations. We integrate the channel attention module into the SteganoGAN as described in the paper of ChatGAN. All models are trained using the DIV2K dataset with 4 BPP message payload for 20 epochs, with all other configurations remaining unchanged, except for the kernel size of these two models.

## B Selection of Query, Key and Value for GMIF

While it is possible to achieve the message hiding task by using the default configuration of W-MSA, the fusion-related researches in other domain[9, 15, 16] using attention mechanism do not agree on the source of features for the query, key and value. To clarify this question, we conduct several experiments using COCO dataset at 4 BPP message capacity to validate different combinations of query, key, and value, searching for the best combination to achieve higher performance. As shown in Tab. 5, the GMIF, when using message features as a query, fails to conceal the message within the cover image, leading to a mere 50% message accuracy. Despite achieving high PSNR and SSIM values, the model prioritizes reconstructing an exact replica of the cover image over performing the message hiding task. The underlined row in Tab. 5 indicates the final configuration adopted by our paper, *i.e.*, using features from the image as a query and sum of image and message feature as key and value. This combination achieves the best message recovery accuracy and imperceptibility.

Query	Key and Value	ACC	PSNR	SSIM
MSG	MSG+IM	50.00%	168.8	1.0
MSG	IM	99.23%	41.35	0.9863
<u>IM</u>	<u>MSG+IM</u>	<u>99.27%</u>	<u>41.87</u>	<u>0.9877</u>
IM	MSG	99.22%	41.43	0.9863
MSG+IM	MSG+IM	99.07%	41.40	0.9862

Table 5: The comparison between different configurations of GMIF. MSG and IM represent the message feature and image feature respectively. MSG+IM denotes the summation of image and message features. The underline indicates the configuration adopted in our paper.

## C Detailed Configurations of StegaFormer

The message concealment pipeline comprises three OPME modules for order-preserving message encoding. Each OPME consists of one MHSA, with 2 heads. Additionally, there are three GMIF modules to fuse the message-image features. Each GMIF includes one W-MSA, with the number of heads set to 2 and the window size set to 16. Regarding the message recovery pipeline, there are four W-MSA modules, all configured to 16 window size and 2 attention heads. Furthermore, one OPMD serving as the message head for recovering the secret message in the message recovery process. The number of heads is set to 2 for MHSA inside OPMD. The detailed configuration of the message recovery pipeline is listed in Tab. 6.

The number of parameters in StegaFormer is solely determined by the length of message segment  $L_{ms}$ . As mentioned in the main paper, the typical settings for  $L_{ms}$  are 16, 32, 48, and 64. On the other hand, increasing the range of message element  $N_r$  does not affect the number of parameters in StegaFormer. The typical number of parameters for our StegaFormer at different values of  $L_{ms}$  are listed in Tab. 7. We also list the Flops and number of parameters at typical 1 BPP in Tab. 8.

There are two approaches to increase the message hiding capacity in our method: increasing the length of message segments  $L_{ms}$  and expanding the range of message elements  $N_r$ . When  $N_r = 1$ , typical choices for  $L_{ms}$  include 16, 32, 48, and 64, corresponding to message capacities of 1, 2, 3, and 4 BPP, respectively.  $N_r$  can also be increased to achieve

higher message capacities. For example,  $N_r = 2^i - 1$ , where  $i = 2, 3, 4$ , represents 2, 3, and 4 bits per message element, respectively. Combining these two factors can lead to a higher message capacity for our models.

We list the experiment results related to different configurations of  $L_{ms}$  and  $N_r$  we have tested in searching for maximum message capacity in Tab. 9 and underlined the listed combinations in the main paper. All the experiments are trained with COCO dataset.

Module Name	Sub Module	Number of Layers	Number of Heads	Window Size	Output Feature Dimension
W-MSA 1	NA	1	2	16	$2 \times L_{ms}$
W-MSA 2	NA	1	2	16	$4 \times L_{ms}$
W-MSA 3	NA	1	2	16	$8 \times L_{ms}$
W-MSA 4	NA	1	2	16	$8 \times L_{ms}$
OPMD	MHSA	1	2	NA	$8 \times L_{ms}$
	MLP	1	NA	NA	$L_{ms}$

Table 6: Detailed configurations for message recovery pipeline. The number added to W-MSA represents the order of W-MSA in the message recovery process from right to left. NA denotes not available.

$(L_{ms}, N_r)$	Capacity	Encoder	Decoder	$(L_{ms}, N_r)$	Capacity	Encoder	Decoder	$(L_{ms}, N_r)$	Capacity	Encoder	Decoder
(16, 1)	1 BPP	10.75M	2.39M	(48, 1)	3 BPP	48.25M	10.70M	(48, 3)	6 BPP	48.25M	10.70M
(32, 1)	2 BPP	21.46M	4.76M	(64, 1)	4 BPP	85.75M	19.00M	(32, 15)	8 BPP	21.46M	4.76M

Table 7: Number of parameters of StegaFormer from 1 to 8 BPP message capacity. M denotes a million parameters.

Method	FLOPs (G)	# Param (M)
StegaFormer	74.3	13.14
Message Concealment of StegaFormer	58.7	10.75
Message Recovery of StegaFormer	15.6	2.39

Table 8: Flops and number of parameters of StegaFormer in 1 BPP message capacity.

Configuration list					Configuration list				
$(L_{ms}, N_r)$	BPP	ACC	PSNR	SSIM	$(L_{ms}, N_r)$	BPP	ACC	PSNR	SSIM
(16,1)	<u>1</u>	<u>99.95%</u>	<u>47.83</u>	<u>0.9969</u>	(16,7)	3	98.72%	42.86	0.9890
(32,1)	<u>2</u>	<u>99.85%</u>	<u>45.30</u>	<u>0.9943</u>	(32,7)	6	95.03%	36.72	0.9673
(48,1)	<u>3</u>	<u>99.68%</u>	<u>43.37</u>	<u>0.9914</u>	(48,7)	9	78.45%	35.50	0.9432
(64,1)	<u>4</u>	<u>99.27%</u>	<u>41.87</u>	<u>0.9877</u>	(16,15)	4	96.32%	40.33	0.9799
(16,3)	2	99.61%	44.98	0.9934	(32,15)	<u>8</u>	<u>91.78%</u>	<u>34.70</u>	<u>0.9508</u>
(32,3)	4	97.46%	41.37	0.9847	(48,15)	12	66.31%	30.37	0.8673
(48,3)	<u>6</u>	<u>95.65%</u>	<u>40.37</u>	<u>0.9803</u>					

Table 9: The experiment results of StegaFormer using different configurations of  $L_{ms}$  and  $N_r$ . The selected configurations are underlined.

## D Detailed Configurations of Experiments

The training process of our model consists of 100,000 iterations, with a batch size of 2. We set  $\lambda_1 = 1 \times 10^{-4}$  and  $\lambda_2 = 1 \times 10^{-6}$  to balance different losses. For comparison, we set the image size to  $256 \times 256$  for all models. All other settings remain as in the officially released models. We utilize the official models of SteganoGAN and LISO [14] since they are publicly



available. We use our own implementation of ChatGAN based on SteganoGAN since there is no officially released code.

## E More Qualitative Examples

More qualitative comparisons of residual and stego image generated by StegaFormer and other two methods are in Fig. 8. Additionally, more comparisons of residual and stego images generated by StegaFormer at different message capacities are in Fig. 9.

## F Experiments of Steganalysis

As described in Sec. 4.3. We conduct steganalysis experiments using SiaStegNet [62]. Among all the experiments, we use COCO dataset for this experiments. We generate 25,000 training sets consisting of cover-stego image pairs and 500 testing pairs using listed approaches and our model. SiaStegNet is trained for 2 epochs. We do not continue training SiaStegNet for more epochs since the Siamese approach is highly effective when cover and stego image pairs are available for training. Training for more than 2 epochs would result in a 100% detection rate for all the methods. The aim of this experiment is to demonstrate the superiority of security of our approach.

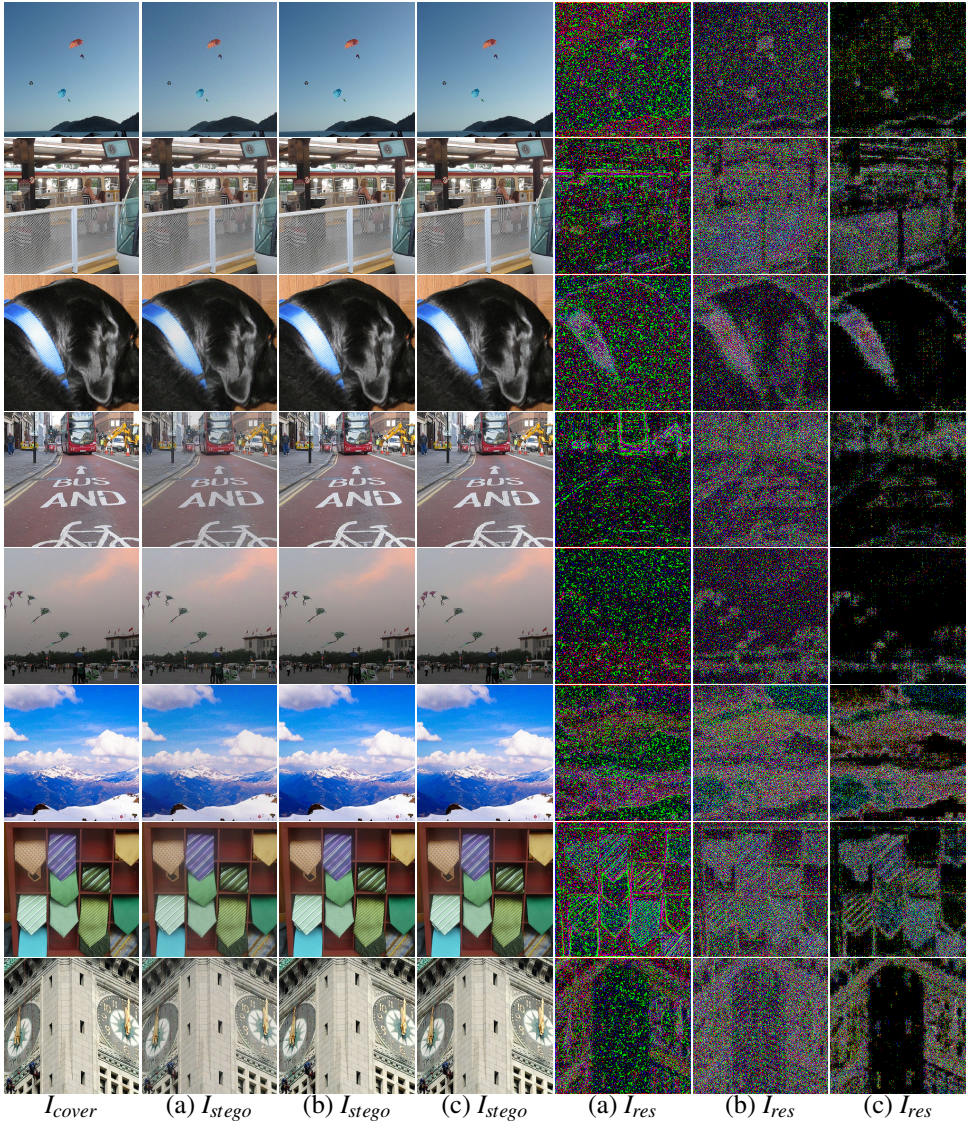


Figure 8: Qualitative results of 3 BPP message hiding using different methods: (a) SteganoGAN, (b) ChatGAN and (c) Ours.  $I_{cover}$ ,  $I_{stego}$  and  $I_{res}$  represent cover image, stego image and residual image respectively. To enhance visualization, the residual images are multiplied by 5. Best viewed in digital version.

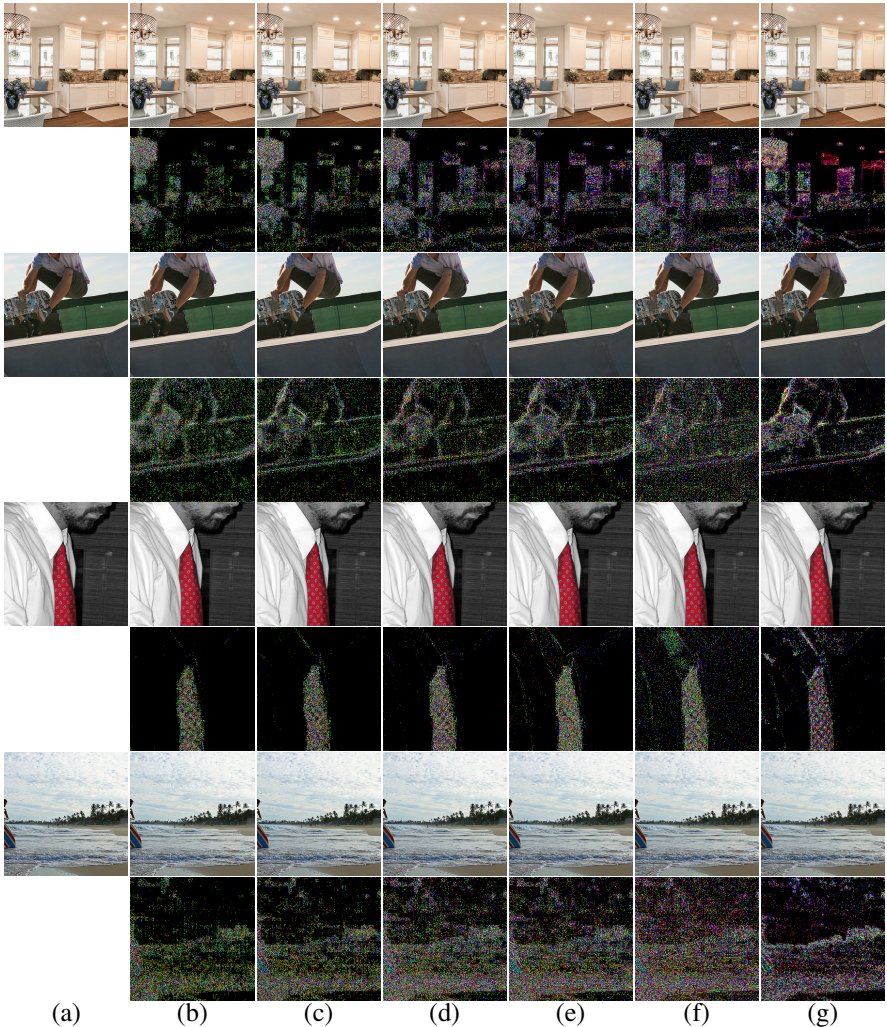


Figure 9: Qualitative results of StegaFormer: (a) cover images  $I_{cover}$ , (b) 1 BPP, (c) 2 BPP, (d) 3 BPP, (e) 4 BPP, (f) 6 BPP, and (g) 8 BPP. Rows 1, 3, 5, and 7, along with columns (b) to (g), represent the stego images  $I_{stego}$ . Rows 2, 4, 6, and 8, along with columns (b) to (g), represent the residual images  $I_{res}$ . To enhance visualization, the residual images are multiplied by 5. Best viewed in digital version.